



# CHORUS

This is the accepted manuscript made available via CHORUS. The article has been published as:

## Formation of Feshbach molecules in the presence of artificial spin-orbit coupling and Zeeman fields

Doga Murat Kurkcuoglu and C. A. R. Sá de Melo

Phys. Rev. A **93**, 023611 — Published 5 February 2016

DOI: [10.1103/PhysRevA.93.023611](https://doi.org/10.1103/PhysRevA.93.023611)

# Formation of Feshbach molecules in the presence of artificial spin-orbit coupling and Zeeman fields

Doga Murat Kurkcuoglu and C. A. R. Sá de Melo  
*School of Physics, Georgia Institute of Technology, Atlanta, 30332, USA*

We derive general conditions for the emergence of singlet Feshbach molecules in the presence of artificial Zeeman fields for arbitrary mixtures of Rashba and Dresselhaus spin-orbit coupling in two or three dimensions. We focus on the formation of two-particle bound states resulting from interactions between ultra-cold spin-1/2 fermions, under the assumption that interactions are short-ranged and occur only in the s-wave channel. In this case, we calculate explicitly binding energies of Feshbach molecules, bound state energy thresholds and analyze their dependence on spin-orbit couplings, Zeeman fields, interactions and center of mass momentum, paying particular attention to the experimentally relevant case of spin-orbit couplings with equal Rashba and Dresselhaus (ERD) amplitudes.

PACS numbers: 67.85.Lm, 03.75.Ss

## I. INTRODUCTION

The effects of spin-orbit interactions are ubiquitous in nature, from the macroscopic scale of the Earth-Moon complex in astronomy and astrophysics, to the microscopic scale of the electron-proton system (Hydrogen atom) in atomic physics. The interest in spin-orbit coupled systems has been revived in condensed matter physics due the emergence of non-trivial topological properties of insulators and superconductors subject to Rashba spin-orbit fields [1, 2], and in atomic physics due to the creation of artificial spin-orbit coupling in ultra-cold atoms [3], which made possible the study of special quantum phase transitions in bosonic systems.

This new tool in the toolbox of atomic physics was experimentally developed first to study interacting bosonic atoms where an equal Rashba-Dresselhaus (ERD) artificial spin-orbit coupling was created [3]. It was suggested that interacting fermions could be studied using the same technique [3, 4], by using the hyperfine states of the fermionic isotope of a neutral atom as the spin labels. Stimulated by the dense literature of the effects of Rashba spin-orbit coupling (SOC) encountered in condensed matter physics [1, 2], several theoretical groups investigated the effects of Rashba SOC for interacting ultra-cold fermions using mean field theories [5–8] or for interacting bosons [9, 10]. Unfortunately, the experimental study of Rashba SOC requires more lasers and further developments are necessary to overcome several difficulties [11]. Thus, presently, artificial Rashba SOC has not yet been created in the context of ultra-cold atoms. However, simultaneous theoretical studies of superfluidity for the experimentally relevant ERD spin-orbit coupling were performed for ultra-cold bosons by others [12, 13] and for ultra-cold fermions by our group [14–16].

One of the benchmarks of experimental studies of Fermi superfluidity of cold atoms without artificial spin-orbit coupling was the emergence of molecular bound states via the use of Feshbach resonances [17], which lead to the formation of molecules [18] and their posterior

Bose-Einstein condensation in  $^{40}\text{K}_2$  [19] and  $^6\text{Li}_2$  [20]. In most of the published literature of ultra-cold fermions with spin-orbit coupling, only non-interacting systems have been investigated [21, 22]. However, recently, the NIST group [23] has demonstrated experimentally the formation of Feshbach molecules of ultra-cold fermions ( $^{40}\text{K}$ ) in the presence of artificial SOC. This observation was also made independently by another group [24]. Our theoretical results were posted [25] simultaneously with the NIST experiment [23], and showed excellent agreement with experimental findings.

The remainder of the paper is organized as follows. In Sec. II, we construct the Hamiltonian for two spin-1/2 fermions in the presence of arbitrary two-dimensional spin-orbit coupling fields, where fermions interact only via local attractive s-wave interactions. We emphasize the importance of choosing the best basis functions to describe the Hamiltonian, and discuss first the limiting case of two non-interacting fermions. In Sec. III, using the momentum representation, we write the Schroedinger's equation in the singlet-triplet basis. In two or three spatial dimensions, we obtain an integral equation for the energy of two-body bound states as a function of center of mass (CM) momentum for arbitrary spin-orbit coupling. We discuss in detail the emergence of two-body bound states (Feshbach molecules) with ERD spin-orbit coupling in three spatial dimensions, since this case was investigated in recent experiments [23, 24]. Our analysis two-body bound states includes the cases of zero and finite CM momentum. We find that when the Zeeman field is transverse to spin-orbit field, the energy of Feshbach molecules is even with respect to the CM momentum, and possesses a minimum when the CM momentum is zero. However, when the Zeeman field has a component along the spin-orbit field, the energy of Feshbach molecules does not have well defined parity with respect to the CM momentum, and for sufficiently large Zeeman field the minimum allowed bound state energy occurs at finite CM momentum. Finally, in Sec. V, we review our main conclusions and make our final comments.

## II. HAMILTONIAN

To address the important issue of the emergence of Feshbach molecules for interacting fermions in the presence of artificial SOC and Zeeman fields, we start from the Hamiltonian for two non-interacting fermions

$$H_0 = H_1 + H_2, \quad (1)$$

written as the sum of two particle contributions, which have the generic form (with  $\hbar = 1$ )

$$H_j = \frac{\hat{\mathbf{k}}_j^2}{2m} - (\mathbf{h}_{R_j} + \mathbf{h}_{D_j}) \cdot \boldsymbol{\sigma}_j - \mathbf{h} \cdot \boldsymbol{\sigma}_j, \quad (2)$$

where  $j = 1, 2$  labels the particle number. The term containing

$$\mathbf{h}_{R_j} = v_R (\hat{k}_{x_j} \mathbf{e}_y - \hat{k}_{y_j} \mathbf{e}_x) \quad (3)$$

represents the Rashba spin-orbit field operator in momentum space, while the term containing

$$\mathbf{h}_{D_j} = v_D (\hat{k}_{x_j} \mathbf{e}_y + \hat{k}_{y_j} \mathbf{e}_x) \quad (4)$$

represents the Dresselhaus spin-orbit field operator. The term containing  $\mathbf{h} = h_x \mathbf{e}_x + h_y \mathbf{e}_y + h_z \mathbf{e}_z$  represents the Zeeman field with components  $h_x = 0$ ,  $h_y = -\delta/2$  (describing the detuning  $\delta$ ) and  $h_z = -\Omega_R/2$  (describing the Raman intensity  $\Omega_R$ ). All these fields are written in energy units. In addition,  $\hat{\mathbf{k}}_j = -i\nabla_j$  is the momentum operator  $\boldsymbol{\sigma}_j = \sigma_{x_j} \mathbf{e}_x + \sigma_{y_j} \mathbf{e}_y + \sigma_{z_j} \mathbf{e}_z$  is the vector Pauli matrix of the  $j^{th}$  particle.

The interaction Hamiltonian considered is

$$H_I(\mathbf{r}_1, \mathbf{r}_2) = -g\delta(\mathbf{r}_1 - \mathbf{r}_2)\delta_{s_1+s_2,0} \quad (5)$$

and describes zero-ranged attractive s-wave interactions between fermions with opposite spins  $s_1 = -s_2$ , or more explicitly using Dirac's bracket (matrix) notation

$$\mathbf{H}_I(\mathbf{r}_1, \mathbf{r}_2) = -g\delta(\mathbf{r}_1 - \mathbf{r}_2)|0,0\rangle\langle 0,0|, \quad (6)$$

where we used the notation  $|0,0\rangle = \frac{1}{\sqrt{2}}(|\uparrow_1\downarrow_2\rangle - |\downarrow_1\uparrow_2\rangle)$  to indicate the singlet state  $|S=0, m_s=0\rangle$  for the two particles labeled by 1 and 2. We use the convention that the first entry for the spin state on the right hand side of the last relation represents particle 1 and the second entry represents particle 2. In the case of three spatial dimensions, the bare coupling constant  $g$  is renormalized through the use of the Lippman-Schwinger relation

$$\frac{L^3}{g} = -\frac{m}{4\pi a_s} + \sum_k \frac{1}{2\epsilon_k}, \quad (7)$$

where  $L^3$  is the volume,  $a_s = a_{bg} [1 + \Delta B/(B - B_0)]$  is the s-wave scattering length expressed in terms of the background scattering length  $a_{bg}$ , the real magnetic field

$B$ , the width  $\Delta B$  of the Feshbach resonance, and the field  $B_0$ , where the resonance is located. While in the two-dimensional case, the bare coupling constant  $g$  is eliminated in favor of the bare binding energy  $E_{bs}$  via

$$\frac{L^2}{g} = \sum_{\mathbf{k}} \frac{1}{2\epsilon_{\mathbf{k}} - E_{bs}}, \quad (8)$$

where  $L^2$  is the area of the system.

Having described the two-particle Hamiltonian operator in terms of kinetic, spin-orbit, Zeeman and interaction energies, we discuss next the choice of an appropriate basis to investigate the formation of Feshbach molecules, when spin-orbit coupling is present.

### A. Choice of Basis

The Hamiltonian described in Eq. (1) can be represented as  $4 \times 4$  matrix in the two-particle spin basis

$$|\Psi\rangle = [|\uparrow_1\uparrow_2\rangle, |\uparrow_1\downarrow_2\rangle, |\downarrow_1\uparrow_2\rangle, |\downarrow_1\downarrow_2\rangle] \quad (9)$$

However, this basis is not the best to work with since the interaction term only contains a singlet s-wave component. Therefore, we rotate  $|\Psi\rangle$  into the singlet-triplet basis

$$|\Phi\rangle = [ |1, +1\rangle, |1, 0\rangle, |1, -1\rangle, |0, 0\rangle ], \quad (10)$$

where the first index represents the total spin  $S$  of the two-particles and the second index indicates the total spin-projection  $m_s$ . Therefore, each entry in  $|\Phi\rangle$  has the form  $|S, m_s\rangle$ . The connection between the two basis is given by the relations  $|1, +1\rangle = |\uparrow_1\uparrow_2\rangle$ , corresponding to the  $S = 1, m_s = +1$  state;  $|1, 0\rangle = \frac{1}{\sqrt{2}}(|\uparrow_1\downarrow_2\rangle + |\downarrow_1\uparrow_2\rangle)$  corresponding to the  $S = 1, m_s = 0$  state;  $|1, -1\rangle = |\downarrow_1\downarrow_2\rangle$ , corresponding to the  $S = 1, m_s = -1$  state; and  $|0, 0\rangle = \frac{1}{\sqrt{2}}(|\uparrow_1\downarrow_2\rangle - |\downarrow_1\uparrow_2\rangle)$  corresponding to the  $S = 0, m_s = 0$  state.

Next, we transform our non-interacting Hamiltonian  $H_0$  into relative momentum  $\mathbf{k} = (\mathbf{k}_1 - \mathbf{k}_2)/2$ , and center of mass (CM) momentum  $\mathbf{K} = \mathbf{k}_1 + \mathbf{k}_2$  coordinates and perform the rotation to the singlet-triplet basis leading to the non-interacting Hamiltonian matrix

$$\mathbf{H}_0 = \begin{pmatrix} \epsilon_{1,2} - 2h_z & -h_{1,2}^{(s)*} & 0 & -h_{1,2}^{(d)*} \\ -h_{1,2}^{(s)} & \epsilon_{1,2} & -h_{1,2}^{(s)*} & 0 \\ 0 & -h_{1,2}^{(s)} & \epsilon_{1,2} + 2h_z & -h_{2,1}^{(d)} \\ -h_{1,2}^{(d)} & 0 & -h_{2,1}^{(d)*} & \epsilon_{1,2} \end{pmatrix}, \quad (11)$$

where  $\epsilon_{1,2} \equiv \epsilon_{1,2}(\mathbf{k}, \mathbf{K}) = \epsilon_{\mathbf{k}_1} + \epsilon_{\mathbf{k}_2}$  is the sum of the kinetic energy of the two particles,

$$h_{1,2}^{(s)} = h_{1,2}^{(s)}(\mathbf{k}, \mathbf{K}) = \frac{1}{\sqrt{2}} [(h_{x_1} + h_{x_2}) + i(h_{y_1} + h_{y_2})] \quad (12)$$

is the scaled sum of the transverse fields felt by both particles,

$$h_{1,2}^{(d)} = h_{1,2}^{(d)}(\mathbf{k}, \mathbf{K}) = \frac{1}{\sqrt{2}} [(h_{x_2} - h_{x_1}) + i(h_{y_2} - h_{y_1})] \quad (13)$$

and its index-exchanged counterpart

$$h_{2,1}^{(d)} = h_{2,1}^{(d)}(\mathbf{k}, \mathbf{K}) = \frac{1}{\sqrt{2}} [(h_{x_1} - h_{x_2}) + i(h_{y_1} - h_{y_2})] \quad (14)$$

are scaled differences of the transverse fields felt by both particles. Notice that  $h_{1,2}^{(d)} = -h_{2,1}^{(d)}$ , and that  $h_{\eta_j}$  represents the transverse field for  $j^{\text{th}}$  particle with  $\eta = x, y, z$ .

More explicitly, we can write the sum of the kinetic energy of the two particles as

$$\epsilon_{1,2}(\mathbf{k}, \mathbf{K}) = k^2/m + K^2/(4m), \quad (15)$$

the matrix element from total spin projection  $m_s = 0 \rightarrow m_s = 1$  or  $m_s = -1 \rightarrow m_s = 0$  in the triplet sector as

$$h_{1,2}^{(s)} = [\beta K_y + i(2h_y + \gamma K_x)]/\sqrt{2}, \quad (16)$$

the matrix element that couples the singlet ( $S = 0$ ) and triplet ( $S = 1$ ) sectors with changes in total spin projection from  $m_s = 0 \rightarrow m_s = 1$

$$h_{1,2}^{(d)} = -\sqrt{2}\beta k_y - i\sqrt{2}\gamma k_x, \quad (17)$$

and the one with changes from  $m_s = 0 \rightarrow m_s = -1$  as

$$h_{2,1}^{(d)} = \sqrt{2}\beta k_y + i\sqrt{2}\gamma k_x. \quad (18)$$

The variables  $\gamma$  and  $\beta$  are defined in terms of the Rashba ( $v_R$ ) and Dresselhaus ( $v_D$ ) coefficients defined in Eqs. (3) and (4) as  $\gamma = v_D + v_R$  and  $\beta = v_D - v_R$ .

Notice that the Hamiltonian matrix  $\mathbf{H}_0$  is not Galilean invariant, and that  $h_{1,2}^{(s)}$  depends only on the CM momentum  $\mathbf{K}$ , while  $h_{1,2}^{(d)}$  and  $h_{2,1}^{(d)}$  depend only on the relative momentum  $\mathbf{k}$ , however the CM and relative coordinates remain coupled. Furthermore, in the experimentally relevant ERD case the parameters the momentum dependence of the fields  $h_{1,2}^{(s)}$ ,  $h_{1,2}^{(d)}$  and  $h_{2,1}^{(d)}$  simplifies dramatically since  $v_D = v_R = v/2$  leads to  $\beta = 0$  and  $\gamma = v$ . In the ERD case, these fields depend on relative or CM momenta only along the  $x$ -direction.

Now that we have discussed our choice of basis and the matrix elements that are present in our Hamiltonian, we discuss next the eigenvalues of two particles in the presence of Zeeman and spin-orbit fields but in the limit of no interactions. This analysis provides the reference energies below which bound states emerge.

## B. Non-interacting limit

The Hamiltonian matrix  $\mathbf{H}_0$  can be diagonalized analytically, and possesses eigenenergies  $E_{\alpha\beta}(\mathbf{k}, \mathbf{K})$ , which

can be written in terms of the two-particle kinetic energy  $\epsilon_{1,2}(\mathbf{k}, \mathbf{K})$  and the effective fields  $h^{(s)}(\mathbf{k}, \mathbf{K}) = |h(\mathbf{k}_1)| + |h(\mathbf{k}_2)|$ , and  $h^{(d)}(\mathbf{k}, \mathbf{K}) = |h(\mathbf{k}_1)| - |h(\mathbf{k}_2)|$ , where  $|h(\mathbf{k}_i)| = \sqrt{h_x^2(\mathbf{k}_i) + h_y^2(\mathbf{k}_i) + h_z^2(\mathbf{k}_i)}$  is the magnitude of the total field (spin-orbit and Zeeman) felt by the  $j^{\text{th}}$  particle. The momenta are  $\mathbf{k}_1 = \mathbf{k} + \mathbf{K}/2$  and  $\mathbf{k}_2 = -\mathbf{k} + \mathbf{K}/2$ . The eigenenergies for two free fermions are

$$E_{\uparrow\uparrow}(\mathbf{k}, \mathbf{K}) = \epsilon_{1,2}(\mathbf{k}, \mathbf{K}) - h^{(s)}(\mathbf{k}, \mathbf{K}) \quad (19)$$

for the lowest energy state,

$$E_{\uparrow\downarrow}(\mathbf{k}, \mathbf{K}) = \epsilon_{1,2}(\mathbf{k}, \mathbf{K}) - h^{(d)}(\mathbf{k}, \mathbf{K}) \quad (20)$$

and its corresponding particle-labeling ( $1 \leftrightarrow 2$ ) image

$$E_{\downarrow\uparrow}(\mathbf{k}, \mathbf{K}) = \epsilon_{1,2}(\mathbf{k}, \mathbf{K}) + h^{(d)}(\mathbf{k}, \mathbf{K}) \quad (21)$$

for the intermediate energies states and

$$E_{\downarrow\downarrow}(\mathbf{k}, \mathbf{K}) = \epsilon_{1,2}(\mathbf{k}, \mathbf{K}) + h^{(s)}(\mathbf{k}, \mathbf{K}) \quad (22)$$

for the highest energy state.

From now, we use the recoil energy  $E_R = k_R^2/(2m)$  as unit of energy and the recoil momentum  $k_R = 2\pi/\lambda$  as unit of momentum, where  $\lambda$  is the wavelength of the laser light used in the Raman beams [3].

In Fig. 1, we show the plots of the generalized two-particle helicity bands  $E_{\uparrow\uparrow}(\mathbf{k}, \mathbf{K})$  (black solid),  $E_{\uparrow\downarrow}(\mathbf{k}, \mathbf{K})$  (red dot-dashed),  $E_{\downarrow\uparrow}(\mathbf{k}, \mathbf{K})$  (green dashed), and  $E_{\downarrow\downarrow}(\mathbf{k}, \mathbf{K})$  (blue dotted) along the direction of relative momentum  $\mathbf{k} = (k_x, 0, 0)$ , for ERD spin-orbit coupling  $v = k_R/m$ , various values of detuning  $h_y$  and Raman intensity  $h_z$ , and specific values of the center of mass momentum  $\mathbf{K} = (K_x, 0, 0)$ .

In Fig. 1a) the parameters used are  $h_y = 0$ ,  $h_z = 0.5E_R$ , and  $K_x = 0$ , which lead to the double well structure in  $E_{\uparrow\uparrow}(\mathbf{k}, \mathbf{K})$  (black solid) due to the ERD spin-orbit orbit momentum shift and Zeeman splitting caused by  $h_z$ . The intermediate energies  $E_{\uparrow\downarrow}(\mathbf{k}, \mathbf{K})$  (red dot-dashed),  $E_{\downarrow\uparrow}(\mathbf{k}, \mathbf{K})$  (green dashed) are degenerate when  $h_y = 0$  with a minimum at  $(0, 0, 0)$ . While the highest energy  $E_{\downarrow\downarrow}(\mathbf{k}, \mathbf{K})$  (blue dotted) is pushed up by the presence of a finite Zeeman field  $h_z$ .

In Fig. 1b) the parameters used are  $h_y = 0.5E_R$ ,  $h_z = 1.0E_R$ , and  $K_x = 0$ , which still lead to a double well structure in  $E_{\uparrow\uparrow}(\mathbf{k}, \mathbf{K})$  (black solid) due to the ERD spin-orbit orbit momentum shift and Zeeman splitting caused by  $h_z$  and  $h_y$ . The intermediate energies  $E_{\uparrow\downarrow}(\mathbf{k}, \mathbf{K})$  (red dot-dashed),  $E_{\downarrow\uparrow}(\mathbf{k}, \mathbf{K})$  (green dashed) are no longer degenerate since  $h_y \neq 0$  and the minima of the one of the bands shift to finite  $(k_x, 0, 0)$ , while for the other it remains at  $(0, 0, 0)$ . Notice that the highest energy  $E_{\downarrow\downarrow}(\mathbf{k}, \mathbf{K})$  (blue dotted) is pushed further up by the presence of finite Zeeman fields  $h_z$  and  $h_y$ .

In Fig. 1c) the parameters used are  $h_y = 1.25E_R$ ,  $h_z = 0.5E_R$ , and  $K_x = 0$ , which no longer lead to a double well structure in  $E_{\uparrow\uparrow}(\mathbf{k}, \mathbf{K})$  (black solid), because the Zeeman splitting caused by  $h_z$  and  $h_y$  is too

large. The minimum value is now located at  $(0, 0, 0)$ . The intermediate energies  $E_{\uparrow\downarrow}(\mathbf{k}, \mathbf{K})$  (red dot-dashed),  $E_{\downarrow\uparrow}(\mathbf{k}, \mathbf{K})$  (green dashed) continue to be non-degenerate since  $h_y \neq 0$  and the minima of one of the bands shift further away from  $(0, 0, 0)$ , while for the other band the minimum remains at  $(0, 0, 0)$ . Notice that the highest energy  $E_{\downarrow\downarrow}(\mathbf{k}, \mathbf{K})$  (blue dotted) is pushed further up by the additional increase in  $h_y$ .

In Fig. 1d) the parameters used are  $h_y = 0.5E_R$ ,  $h_z = 0.5E_R$ , and  $K_x = 1.25k_R$ , which also do not lead to a double well structure in  $E_{\uparrow\uparrow}(\mathbf{k}, \mathbf{K})$  (black solid), because the splitting caused  $K_x$  is too large. Recall that for the field  $h_{1,2}^{(s)}$  defined in Eq. (16) the effect of finite and positive  $K_x$  is similar to that of an increased  $h_y$ , since they enter in  $h_{1,2}^{(s)}$  as the combination  $2h_y + \gamma K_x$ . The minimum value is again located at  $(0, 0, 0)$ . The intermediate energies  $E_{\uparrow\downarrow}(\mathbf{k}, \mathbf{K})$  (red dot-dashed),  $E_{\downarrow\uparrow}(\mathbf{k}, \mathbf{K})$  (green dashed) continue to be non-degenerate since  $h_y \neq 0$  and the minima of one of the bands continue to be at finite  $(k_x, 0, 0)$ , while for the other band the minimum remains at  $(0, 0, 0)$ . Notice that the highest energy  $E_{\downarrow\downarrow}(\mathbf{k}, \mathbf{K})$  (blue dotted) is pushed further up (out of range) by the combined largeness of  $2h_y + \gamma K_x$ . Recall that in the ERD case  $\gamma = v = k_R/m$ , thus when  $K_x = 1.25k_R$ , the product  $vK_x = 1.25k_R^2/m = 2.5E_R$ , when written in terms of the recoil energy  $E_R$ .

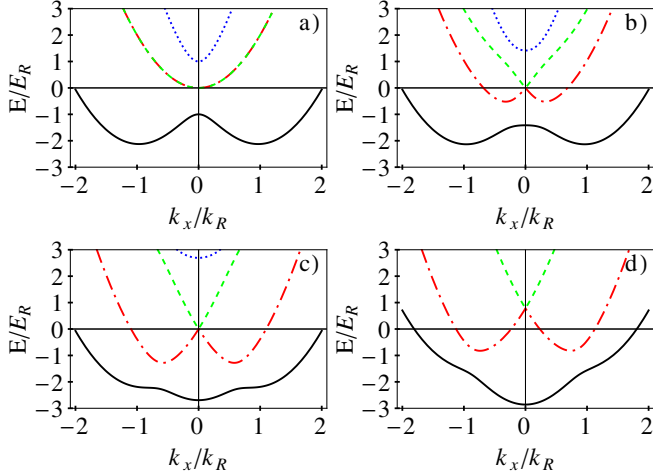


FIG. 1: (color online) Plots of the generalized two-particle helicity bands  $E_{\uparrow\uparrow}(\mathbf{k}, \mathbf{K})$  (black solid),  $E_{\uparrow\downarrow}(\mathbf{k}, \mathbf{K})$  (red dot-dashed),  $E_{\downarrow\uparrow}(\mathbf{k}, \mathbf{K})$  (green dashed), and  $E_{\downarrow\downarrow}(\mathbf{k}, \mathbf{K})$  (blue dotted) along the direction of relative momentum  $\mathbf{k} = (k_x, 0, 0)$ , for ERD spin-orbit coupling  $v = k_R/m$ , various values of detuning  $h_y$  and Raman intensity  $h_z$ , and specific values of the center of mass momentum  $\mathbf{K} = (K_x, 0, 0)$ . The parameters used are a)  $h_y = 0$ ,  $h_z = 0.5E_R$ , and  $K_x = 0$ ; b)  $h_y = 0.5E_R$ ,  $h_z = 1.0E_R$ , and  $K_x = 0$ ; c)  $h_y = 1.25E_R$ ,  $h_z = 0.5E_R$ , and  $K_x = 0$ ; and d)  $h_y = 0.5E_R$ ,  $h_z = 0.5E_R$ , and  $K_x = 1.25k_R$ . Notice the change in location of the minimum of  $E_{\uparrow\uparrow}$  from finite  $k_x$  in a) and b) to  $k_x = 0$  in c) and d).

These unbound two-particle energies are important because they serve as reference energies when two-particle

bound states (Feshbach molecules) emerge when interactions are turned on. The formation of Feshbach molecules is energetically favorable when their energy is lower than the minimum of the lowest two-particle energy band  $E_{\uparrow\uparrow}(\mathbf{k}, \mathbf{K})$ . With that in mind, we reintroduce the attractive contact interaction defined in Eq. (6), and discuss next the emergence of Feshbach molecules.

### III. EMERGENCE OF FESHBACH MOLECULES (BOUND STATES)

To write the Schroedinger's equation for two interacting fermions in momentum space, we perform first a Fourier transformation to the interaction Hamiltonian  $\mathbf{H}_I(\mathbf{r}_1, \mathbf{r}_2)$  defined in Eq. (6), and add the Fourier-transformed matrix  $\mathbf{H}_I(\mathbf{k}, \mathbf{K})$  to the non-interacting Hamiltonian matrix  $\mathbf{H}_0(\mathbf{k}, \mathbf{K})$  defined in Eq. (11). This procedure leads to the Schroedinger's equation

$$(\mathbf{H}_0 + \mathbf{H}_I) \Lambda_{\mathbf{k}, \mathbf{K}} = E \mathbf{I} \Lambda_{\mathbf{k}, \mathbf{K}}, \quad (23)$$

where the four-dimensional spinor

$$\Lambda_{\mathbf{k}, \mathbf{K}} = [\Lambda_{1,1}(\mathbf{k}, \mathbf{K}), \Lambda_{1,0}(\mathbf{k}, \mathbf{K}), \Lambda_{1,-1}(\mathbf{k}, \mathbf{K}), \Lambda_{0,0}(\mathbf{k}, \mathbf{K})]^t$$

includes components both in the triplet and singlet sectors. In the triplet sector,  $\Lambda_{1,1}(\mathbf{k}, \mathbf{K})$  corresponds to the component labeled by  $(S = 1, m_s = 1)$ ;  $\Lambda_{1,0}(\mathbf{k}, \mathbf{K})$  corresponds to the component labeled by  $(S = 1, m_s = 0)$ ;  $\Lambda_{1,-1}(\mathbf{k}, \mathbf{K})$  corresponds to the component labeled by  $(S = 1, m_s = -1)$ . While in the singlet sector,  $\Lambda_{0,0}(\mathbf{k}, \mathbf{K})$  corresponds to the component labeled by  $(S = 0, m_s = 0)$ .

The action of the interaction Hamiltonian on the four-dimensional spinor leads to the vector

$$\mathbf{H}_I \Lambda_{\mathbf{k}, \mathbf{K}} = [0, 0, 0, -g \sum_{\mathbf{k}} \Lambda_{0,0}(\mathbf{k}, \mathbf{K})]^t, \quad (24)$$

where  $\sum_{\mathbf{k}}$  represents a summation over the relative momenta  $\mathbf{k}$ . The eigenvalues of Eq. (23) can be found in any dimension by rearranging the Hamiltonian as

$$[E \mathbf{I} - \mathbf{H}_0] \Lambda_{\mathbf{k}, \mathbf{K}} = \mathbf{H}_I \Lambda_{\mathbf{k}, \mathbf{K}} \quad (25)$$

and inverting the matrix  $[E \mathbf{I} - \mathbf{H}_0]$  to obtain the relation

$$\Lambda_{\mathbf{k}, \mathbf{K}} = \frac{\text{Adj}[E \mathbf{I} - \mathbf{H}_0]}{\text{Det}[E \mathbf{I} - \mathbf{H}_0]} \mathbf{H}_I \Lambda_{\mathbf{k}, \mathbf{K}}, \quad (26)$$

where  $\text{Adj}[\mathbf{M}]$  is the adjucate matrix and  $\text{Det}[\mathbf{M}]$  is the determinant of  $\mathbf{M}$ . Here, we used the standard result for the inverse matrix  $\mathbf{M}^{-1} = \text{Adj}[\mathbf{M}]/\text{Det}[\mathbf{M}]$ . Integration over the relative momentum  $\mathbf{k}$  on both sides of Eq. (26) leads to the integral equation

$$\frac{L^d}{g} = - \sum_{\mathbf{k}} \frac{(E - \epsilon_{1,2})(E - \epsilon_{1,2} + |h_t|)(E - \epsilon_{1,2} - |h_t|)}{(E - E_1)(E - E_2)(E - E_3)(E - E_4)}, \quad (27)$$

which is the central result of this paper. From this eigenvalue equation, we can extract the bound state energy  $E_B(\mathbf{K})$  of Feshbach molecules as a function of its center of mass momentum  $\mathbf{K}$ , for varying spin-orbit coupling, Zeeman fields and interaction parameters. Throughout the remainder of this paper, we will be referring back to Eq. (27).

Here, the function  $|h_t| = \sqrt{4h_z^2 + |h_{12s}(\mathbf{k}, \mathbf{K})|^2}$  is the amplitude of the total field  $\mathbf{h}_t = \mathbf{h}_1 + \mathbf{h}_2$ ,  $d$  is the dimension of the system, and  $E_i(\mathbf{k}, \mathbf{K})$  are the eigenvalues of  $\mathbf{H}_0$ , corresponding to the two-particle generalized helicity bands  $E_{\alpha\beta}(\mathbf{k}, \mathbf{K})$ . We identify the right-hand-side of Eq. (27) with the function

$$G_s(E, \mathbf{K}) = \sum_{\mathbf{k}, \alpha, \beta} \frac{|\mathbf{U}_{\alpha\beta, s}(\mathbf{k}, \mathbf{K})|^2}{E - E_{\alpha\beta}(\mathbf{k}, \mathbf{K})}, \quad (28)$$

which corresponds to the spectral representation of the two-body Green's function for non-interacting fermions in the singlet channel of the original spin states ( $\uparrow, \downarrow$ ). Here,  $|\mathbf{U}_{\alpha\beta, s}(\mathbf{k}, \mathbf{K})|^2$  represents the spectral weight in the singlet channel ( $s$ ) associated with the spinor eigenvector  $\mathbf{U}_{\alpha\beta}(\mathbf{k}, \mathbf{K})$  of  $\mathbf{H}_0$  with eigenvalue  $E_{\alpha\beta}(\mathbf{k}, \mathbf{K})$ . No other channel, but the singlet channel contributes to  $G_s(\mathbf{k}, \mathbf{K})$ , as the interactions between fermions are non-zero only between the original  $\uparrow$  and  $\downarrow$  spins.

By ordering the eigenvalues  $E_1 \geq E_2 \geq E_3 \geq E_4$ , a simple inspection of Eq. (27) shows that a necessary condition for the formation of singlet Feshbach molecules occurs when  $E(\mathbf{K}) \leq \min_{\mathbf{k}}\{E_4(\mathbf{k}, \mathbf{K})\}$ , provided that there is spectral weight in the singlet interaction channel for the lowest energy of two free fermions. From Eq. (27), we obtained Feshbach molecule energies  $E = E_B(\mathbf{K})$  for an arbitrary mixture of Rashba and Dresselhaus terms at any value of  $\mathbf{K}$  in 2D and 3D. We also calculated the effective mass tensor and the corresponding Bose-Einstein condensation temperature [25]. However, we show here results only for the ERD case in 3D, because of its experimental relevance for ultra-cold fermions [3]. We parametrize the ERD coupling parameter in terms of the recoil momentum  $k_R$  as  $v = [1 - \cos(\theta)] k_R / (2m)$  for Raman beams that cross at an arbitrary angle  $\theta$ . Current experiments correspond to  $\theta = \pi$  and  $v = k_R/m$ .

We discuss next, the simplest example of formation of Feshbach molecules corresponding to ERD spin-orbit coupling, and bound states with zero center of mass momentum.

### A. Zero Center of Mass Momentum

To gain insight in the ERD case, first we find the energy  $E(\mathbf{K})$  of Feshbach molecules from the integral defined in Eq. (27), for zero CM momentum  $\mathbf{K} = \mathbf{0}$  and zero detuning  $h_y = 0$ , but finite  $h_z$  in three spatial dimensions. In this case, the eigenvalues of the non-interacting Hamiltonian matrix  $\mathbf{H}_0$  take the simple form  $E_{\downarrow\downarrow}(\mathbf{k}, \mathbf{0}) = k^2/m + 2|h_{\text{eff}}(\mathbf{k})|$  for the highest energy,

$E_{\uparrow\downarrow}(\mathbf{k}, \mathbf{0}) = E_{\downarrow\uparrow}(\mathbf{k}, \mathbf{0}) = k^2/m$ , for the intermediate energies, and  $E_{\uparrow\uparrow}(\mathbf{k}, \mathbf{0}) = k^2/m - 2|h_{\text{eff}}(\mathbf{k})|$  for the lowest energy, where the magnitude of the effective field is  $|h_{\text{eff}}(\mathbf{k})| = \sqrt{(vk_x)^2 + h_z^2}$ . The condition for the emergence of zero CM momentum Feshbach molecules is then  $E(\mathbf{K} = \mathbf{0}) \leq \min_{\mathbf{k}}\{E_{\uparrow\uparrow}(\mathbf{k}, \mathbf{0})\}$ .

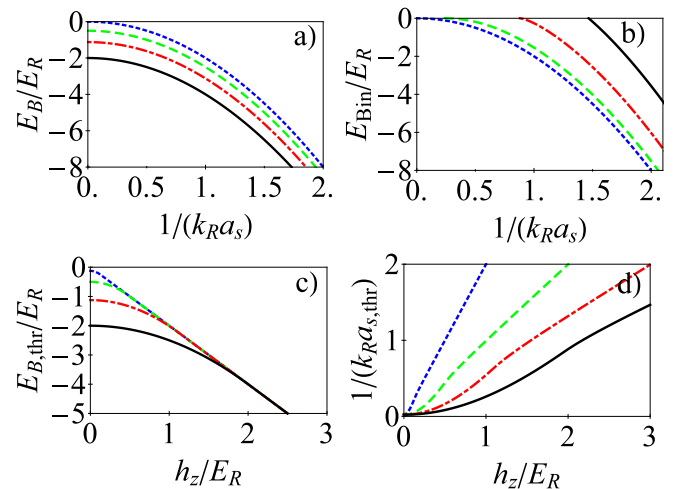


FIG. 2: (color online) Plots of bound state energy  $E_B/E_R$  versus  $1/(k_R a_s)$  with  $\mathbf{K} = \mathbf{0}$ ,  $h_z = 0$ ,  $h_y = 0$  are shown in a) for  $v = 0$  (blue dotted),  $v = 0.5k_R/m$  (green dashed),  $v = 0.75k_R/m$  (red dotdashed), and  $v = k_R/m$  (black solid). Plots of  $E_{Bin}/E_R$  versus  $1/(k_R a_s)$  with  $\mathbf{K} = \mathbf{0}$ ,  $v = k_R/m$ ,  $h_y = 0$  are shown in b) for  $h_z = 0$  (blue dotted),  $h_z = E_R$  (green dashed),  $h_z = 2E_R$  (red dotdashed),  $h_z = 3E_R$  (black solid). Plots of  $E_{B,thr}/E_R$  and  $1/(k_R a_{s,thr})$  versus  $h_z/E_R$  with  $\mathbf{K} = \mathbf{0}$ ,  $h_y = 0$  are shown respectively in c) and d) for  $v = 0.25k_R/m$  (blue dotted),  $v = 0.5k_R/m$  (green dashed),  $v = 0.75k_R/m$  (red dotdashed) and  $v = k_R/m$  (black solid).

In Fig. 2a, we show the bound-state energy  $E = E_B$  of Feshbach molecules (in units of  $E_R$ ) versus the scattering parameter  $1/(k_R a_s)$  at zero CM momentum ( $\mathbf{K} = \mathbf{0}$ ), zero detuning ( $h_y = 0$ ) and in the limit of  $h_z \rightarrow 0$ . In this case, the energy of Feshbach molecules can be obtained analytically as  $E_B(v) = -1/(ma_s^2) - mv^2$ , which means that the existence of spin-orbit coupling lowers the energy of the bound state from the standard value  $E_B(0) = -1/(ma_s^2)$  by the amount  $mv^2$ . The scaled bound state energy is

$$\frac{E_B}{E_R} = -2 \left[ \left( \frac{1}{k_R a_s} \right)^2 + \left( \frac{mv}{k_R} \right)^2 \right] \quad (29)$$

and the plots shown in Fig. 2a reflect this relation. However, notice that the threshold scattering length for the emergence of bound states remains at  $a_s \rightarrow \infty$  or  $1/(k_R a_s) = 0$ .

The binding energy at  $\mathbf{K} = \mathbf{0}$ , defined as  $E_{Bin} = E_B - \min_{\mathbf{k}} E_{\uparrow\uparrow}(\mathbf{k}, \mathbf{K} = \mathbf{0})$  is a better indicator of the effects of spin-orbit coupling since the minimum energy of two free fermions also changes with  $v$ . An example of  $E_{Bin}$  is shown in Fig. 2b, where we plot  $E_{Bin}/E_R$  versus

$1/(k_R a_s)$  for fixed  $v = k_R/m$  and increasing Zeeman field  $h_z$ . As  $h_z$  increases, the threshold interaction parameter for the formation of Feshbach molecules is shifted from positive infinity to finite and positive scattering lengths, indicating that stronger attraction between fermions is necessary to overcome the depairing effects of  $h_z$ .

In Fig. 2c, we show the threshold bound-state energy  $E_{B,th}$  for  $\mathbf{K} = \mathbf{0}$  and  $h_y = 0$  as a function of  $h_z$  and varying  $v$ , obtained from the threshold condition  $E(\mathbf{K}) \leq \min_{\mathbf{k}}\{E_{\uparrow\uparrow}(\mathbf{k}, \mathbf{K})\}$ . For  $\mathbf{K} = \mathbf{0}$ , the  $\min_{\mathbf{k}}\{E_{\uparrow\uparrow}(\mathbf{k}, \mathbf{K} = \mathbf{0})\}$  occurs at non-zero  $k_x$ , when  $|h_z| < mv^2$ , and at  $k_x = 0$  when  $|h_z| \geq mv^2$ . Therefore, for  $|h_z| < mv^2$ , the bound state energy  $E_B$  satisfies the condition  $E_B \leq E_{B,th} = -mv^2 - h_z^2/(mv^2)$ . In this case, it has the dimensionless form  $\tilde{E}_{B,th} = -2\tilde{p}^2 - \tilde{h}_z^2/(2\tilde{p}^2)$ , where  $\tilde{E}_{B,th} = E_{B,th}/E_R$ ,  $\tilde{h}_z = h_z/E_R$ , and  $\tilde{p} = p/k_R$  with  $p = mv$ . However, for  $|h_z| > mv^2$  the bound state energy  $E_B$  satisfies the condition  $E_B \leq E_{B,th} = -2h_z$ , and acquires the dimensionless form  $\tilde{E}_{B,th} = -2\tilde{h}_z$ . This change in behavior of the minimum of  $E_{\uparrow\uparrow}(\mathbf{k}, \mathbf{0})$  is illustrated in Fig. 2c.

In Fig. 2d, we show the threshold scattering length  $a_{s,th}$  as a function of  $h_z$ , which behaves differently as  $h_z$  reaches the critical value  $h_{z,c} = mv^2$ . This condition is expressed in dimensionless units as  $\tilde{h}_{z,c} = 2\tilde{p}^2$ . It is at this critical value that  $E_{\uparrow\uparrow}(\mathbf{k}, \mathbf{0})$  changes from a double minimum when  $|\tilde{h}_z| < \tilde{h}_{z,c}$  to a single minimum when  $|\tilde{h}_z| \geq \tilde{h}_{z,c}$ . For fixed SOC  $v$ , the threshold  $a_{s,th}$  progressively grows with increasing  $h_z$  first quadratically for  $|h_z| < h_{z,c}$  and then linearly for  $|h_z| \geq h_{z,c}$ , as stronger attractive s-wave (singlet) interactions are necessary to overcome the de-pairing effect of  $h_z$  that tends to align the original spins.

We have just discussed the formation of Feshbach molecules at zero center of mass momentum  $\mathbf{K} = \mathbf{0}$  for zero detuning ( $h_y = 0$ ), but non-zero Raman intensity ( $h_z \neq 0$ ). Next, we discuss the solutions of Eq. (27) in three dimensions, for the emergence of Feshbach molecules at  $\mathbf{K} = \mathbf{0}$ , but with both  $h_y \neq 0$  and  $h_z \neq 0$ . The main results are shown in Fig. 3.

In Fig. 3a, we show plots of the energy of Feshbach molecules  $E_B/E_R$  versus interaction parameter  $1/(k_R a_s)$  for  $h_y = 0.25E_R$ ,  $h_z = 0.5E_R$  and changing ERD spin-orbit coupling  $v$ . Notice two trends as a function of  $v$ . The first trend is that binding energies are shifted downwards with increasing  $v$ . The second trend is that the threshold interaction parameter decreases with increasing  $v$  showing that larger SOC facilitates the formation of molecules when Zeeman fields are present.

In Fig. 3b, we show the binding energy  $E_{Bin}/E_R$  versus  $1/(k_R a_s)$  for fixed parameters  $v = k_R/m$ ,  $h_z = E_R$ , and  $\mathbf{K} = \mathbf{0}$ , but changing  $h_y$ . The main information that this figure contains is that the scattering parameter threshold increases with  $h_y$  as a stronger attractive interaction is necessary to form singlet Feshbach molecules in the original spin basis ( $\uparrow, \downarrow$ ).

In Fig. 3c, we show the bound state energy threshold  $E_{B,th}/E_R$  versus  $h_y/E_R$  for fixed parameters  $\mathbf{K} = \mathbf{0}$ ,

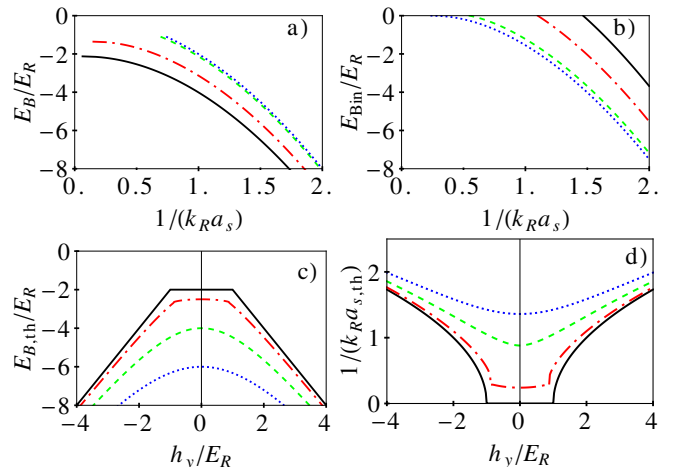


FIG. 3: (color online) a) Plots of  $E_B/E_R$  versus  $1/(k_R a_s)$  with  $\mathbf{K} = \mathbf{0}$ ,  $h_y = 0.25E_R$ , and  $h_z = 0.5E_R$  for  $v = 0.05k_R/m$  (blue dotted),  $v = 0.25k_R/m$  (green dashed),  $v = 0.75k_R/m$  (red dotdashed),  $v = k_R/m$  (black solid). b) Plots of  $E_{Bin}/E_R$  versus  $1/(k_R a_s)$  with  $\mathbf{K} = \mathbf{0}$ ,  $h_z = E_R$ , and  $v = k_R/m$  for  $h_y = 0$  (blue dotted),  $h_y = E_R$  (green dashed),  $h_y = 2E_R$  (red dotdashed),  $h_y = 3E_R$  (black solid). Plots of  $E_{B,th}/E_R$  and  $1/(k_R a_{s,th})$  versus  $h_y/E_R$  with  $\mathbf{K} = \mathbf{0}$ , and  $v = k_R/m$  are shown respectively in c) and d) for  $h_z = 0$  (black solid);  $h_z = E_R$  (red dotdashed);  $h_z = 2E_R$  (green dashed);  $h_z = 3E_R$  (blue dotted).

$v = k_R/m$  and varying Zeeman field strengths of  $h_z = 0, E_R, 2E_R, 3E_R$ . Notice two important trends. First, for fixed  $h_y$ , the larger  $h_z$  then the lower  $E_{B,th}/E_R$ , indicating that it becomes more difficult to form Feshbach molecules with increasing  $h_z$ . Second, for fixed and non-zero  $h_z$ , the larger  $h_y$  then the lower  $E_{B,th}/E_R$ , indicating again that it becomes more difficult to form Feshbach molecules. However, for  $h_z = 0$  there is a range of  $h_y$  fields, where  $E_{B,th}/E_R$  remains constant due to a compensatory effect of the spin-orbit field, before it decreases with increasing  $h_y$ . It is also important to point out that, at zero center of mass momentum ( $\mathbf{K} = \mathbf{0}$ ), the bound state threshold energy is symmetric for  $h_y \rightarrow -h_y$ , as well as for  $h_z \rightarrow -h_z$ .

In Fig. 3d, we show the scattering parameter threshold  $1/(k_R a_{s,th})$  versus  $h_y/E_R$  for fixed parameters  $\mathbf{K} = \mathbf{0}$ ,  $v = k_R/m$  and varying Zeeman field strengths of  $h_z = 0, E_R, 2E_R, 3E_R$ . There are here also two important trends. The first one is that, for fixed  $h_y$ , the threshold  $1/(k_R a_{s,th})$  increases with increasing  $h_z$ . This is a reflection of the requirement of larger attractive s-wave singlet interactions to compensate for the increase in Zeeman energy that makes the formation of bound states in the singlet channel more difficult. The second one is that, for fixed and non-zero  $h_z$ , the larger  $h_y$  the larger  $1/(k_R a_{s,th})$ , indicating again that it becomes more difficult to form Feshbach molecules, because of the associated Zeeman energy cost. However, for  $h_z = 0$  there is a range of  $h_y$  fields, where  $1/(k_R a_{s,th})$  remains constant due to a compensatory effect of the spin-orbit field,

before it increases with increasing  $h_y$ . It is also important to point out that, at zero center of mass momentum  $\mathbf{K} = \mathbf{0}$ , the scattering parameter threshold is symmetric for  $h_y \rightarrow -h_y$ , as well as, for  $h_z \rightarrow -h_z$ .

Having discussed the emergence of Feshbach molecules at zero center of mass momentum ( $\mathbf{K} = \mathbf{0}$ ), we present next the case of Feshbach molecules that are formed with non-zero center of mass momentum ( $\mathbf{K} \neq \mathbf{0}$ ).

## B. Finite Center of Mass Momentum

To find the energy of Feshbach molecules as a function of center of mass momentum  $\mathbf{K}$ , we solve again Eq. (27), which represents the general eigenvalue equation for an arbitrary mixture of Rashba and Dresselhaus terms, with  $\mathbf{K} \neq \mathbf{0}$ . However, we continue to focus on the equal Rashba-Dresselhaus (ERD) regime in three dimensions, given its relevance to current experiments. In this case, the bound state energy  $E_B(\mathbf{K})$  has only a non-trivial dependence on the component  $K_x$  of the center of mass momentum  $\mathbf{K}$ .

In Figs. 4a-d, we show the energy dispersions  $E_B(\mathbf{K})$  of Feshbach molecules and the threshold energy  $E_{B,th} = \min_{\mathbf{k}}\{E_{\uparrow\uparrow}(\mathbf{k}, \mathbf{K})\}$  along CM momentum  $\mathbf{K} = (K_x, 0, 0)$ , with ERD spin-orbit coupling  $v = k_R/m$  and Raman intensity  $h_z = 0.5E_R$ . The threshold energy  $E_{B,th}$  is represented by black solid curves, while the bound state energy  $E_B(\mathbf{K})$  is represented by blue dotted, green dashed and red dotdashed curves for scattering parameters  $1/(k_R a_s) = 0.75, 1.25$ , and  $1.75$ , respectively.

In Fig. 4a, we show the zero detuning result corresponding to  $h_y = 0$ , while in Fig. 4b, Fig. 4c and Fig. 4d, we show non-zero detuning cases corresponding to  $h_y = 0.5E_R, 1.5E_R$ , and  $2.5E_R$ , respectively.

The first thing to notice in Figs. 4a-d is that the binding energy  $E_{Bin}(\mathbf{K}) = E_B(\mathbf{K}) - E_{B,th}(\mathbf{K})$  of Feshbach molecules becomes more negative with increasing interaction parameter, as expected. For instance, look at Fig. 4a or Fig. 4b and follow the trend as one goes from the blue dotted to the green dashed to the red dotdashed lines. It is also important to observe that in Fig. 4a the dispersions are even in  $K_x$  since  $h_y = 0$ , but in Figs. 4b-d parity is lost since  $h_y \neq 0$ . This occurs because the bound state energy  $E_B(\mathbf{K})$  is a function of  $|h_{1,2}^{(s)}|^2$ , where the matrix element  $h_{1,2}^{(s)}$  is defined in Eq. (16). For the ERD case,  $h_{1,2}^{(s)} = i(2h_y + vK_x)/\sqrt{2}$ , and the loss of parity in  $E_B(\mathbf{K})$  happens along the  $K_x$  direction only.

Furthermore, notice that Feshbach molecules are stable only within the range of CM momenta shown by the blue dotted, green dashed and red dotdashed curves in Figs. 4a-d. Outside this region of stability, Feshbach molecules decay into the two-particle continuum due to Landau damping. In addition, when  $h_y$  is positive and increasing, the region of stable Feshbach molecules shifts towards negative CM momenta, such beyond a critical value  $h_{y,c}$  no Feshbach molecules with zero CM momen-

tum are stable for fixed scattering parameter  $1/(k_F a_s)$ . This unusual effect is a direct consequence of the absence of Galilean invariance and the loss of parity introduced by the matrix element  $h_{1,2}^{(s)}$  that couples the center of mass momentum of two fermions and their spins. For instance, to see this trend compare the blue dotted lines corresponding to  $1/(k_F a_s) = 0.75$ , where  $h_y$  is increasing from Fig. 4a to Fig. 4d.

Whenever there is a minimum or a maximum of  $E_B(\mathbf{K})$  as a function of center of mass momentum  $\mathbf{K}$ , it is possible to perform an expansion around this minimum or maximum and define an effective mass for the Feshbach molecule. For instance, in the case of zero detuning ( $h_y = 0$ ), such expansion is always possible and leads to the binding energy

$$E_B(\mathbf{K}) = E_B(\mathbf{0}) + \frac{K_x^2}{2M_x} + \frac{K_y^2}{2M_y} + \frac{K_z^2}{2M_z}, \quad (30)$$

where  $M_x$ ,  $M_y$ , and  $M_z$  are the effective masses of Feshbach molecules along the  $x, y$  and  $z$  directions, respectively.

We discuss briefly the effective masses in two simple limits of the more general mixture of Rashba and Dresselhaus spin-orbit terms: the ERD and the Rashba-only cases. Recalling that  $m$  is the mass of the fermions, in the ERD limit, the masses  $M_y = M_z = 2m$  are unrenormalized by the spin-orbit coupling. However, in general  $M_x \neq 2m$  is renormalized due to the one-dimensional nature of the ERD spin-orbit field. The effective mass  $M_x$  tends to  $2m$  in the limit of  $1/(k_F a_s)$  tending to infinity. On the other hand, in the Rashba-only regime, the mass  $M_z = 2m$  is unrenormalized, while the masses  $M_x = M_y \neq 2m$  are renormalized due to the two-dimensional nature of the Rashba spin-orbit field. The effective masses  $M_x, M_y$  tend to  $2m$  in the limit of  $1/(k_F a_s)$  tending to infinity.

Having discussed the emergence of Feshbach molecules with finite center of mass momentum, and having analysed briefly the anisotropic nature of the effective masses of such molecules when spin-orbit and Zeeman fields are present, next we make some comments regarding Bose-Einstein condensation of Feshbach molecules when their binding energy can be described by Eq. (30).

## IV. BOSE-EINSTEIN CONDENSATION OF FESHBACH MOLECULES

In our investigation, Feshbach molecules emerge as two-body bound states of two fermions, therefore if we consider a gas of dilute and non-interacting molecular bound states with energy dispersion given by Eq. (30), the density of these molecules is

$$n_{bs} = \frac{1}{L^3} \sum_{\mathbf{K}} b(\mathbf{K}), \quad (31)$$

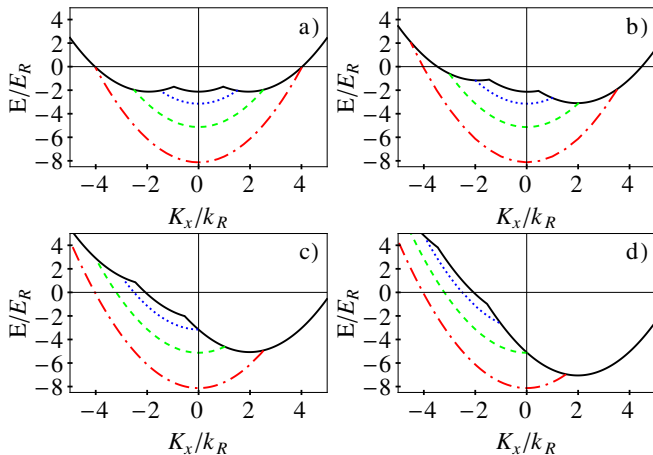


FIG. 4: (color online) Plots of bound state threshold energies (solid black) and of energies of Feshbach molecules (blue dotted with  $1/(k_R a_s) = 0.75$ ; green dashed with  $1/(k_R a_s) = 1.25$ ; red dotdashed with  $1/(k_R a_s) = 1.75$ ) versus center of mass momentum  $\mathbf{K} = (K_x, K_y = 0, K_z = 0)$  for  $v = k_R/m$  and  $h_z = 0.5E_R$ , with a)  $h_y = 0$ ; b)  $h_y = 0.5E_R$ ; c)  $h_y = 1.5E_R$ ; and d)  $h_y = 2.5E_R$ . Notice the absence of inversion symmetry (parity) when  $h_y \neq 0$ .

where  $L^3$  is the volume, and the function

$$b(\mathbf{K}) = \frac{1}{e^{[E_B(\mathbf{K}) - \mu_{bs}] - 1}} \quad (32)$$

is the Bose distribution. When the chemical potential  $\mu_{bs}$  approaches the binding energy  $E_B(\mathbf{0})$ , then the bound states exhibit the phenomenon of Bose-Einstein condensation. The present situation differs slightly from the standard case with dispersion  $E_B(\mathbf{K}) = E_B(\mathbf{0}) + \mathbf{K}^2/(2M)$ , because the masses are anisotropic.

In the isotropic case, when there are no artificial spin-orbit and Zeeman fields, the condensation occurs when  $n_{bs} = CT_{BEC}^{3/2} M^{3/2}$  where the constant  $C = \zeta(3/2)/(2\pi)^{3/2}$  with  $\zeta(3/2) = 2.6124$  being the Riemann zeta function evaluated at  $3/2$ . This constant has numerical value  $C = 0.16587$ , and our analysis leads to the standard BEC temperature

$$T_{BEC}^{iso} = \frac{1}{C^{2/3}} \frac{n_{bs}^{2/3}}{M} \quad (33)$$

for the case of isotropic bound state dispersion. However, since each bound state is formed by two fermions, the density of bound states is half of the fermion density, that is,  $n_{bs} = n_F/2$ , and the mass of the bound state is twice that of the fermion, that is,  $M = 2m$ . These two statements put together lead to the relation  $n_{bs}^{2/3}/M = 2^{-2/3} n_F^{2/3}/(2m)$ , which ultimately produces the condensation temperature

$$T_{BEC}^{iso} = \frac{1}{(2C)^{2/3}} \frac{n_F^{2/3}}{2m} = 0.218 E_F \quad (34)$$

where  $E_F = k_F^2/(2m)$  is the Fermi energy of a non-interacting gas of fermions with two internal spin states, and the density of fermions is  $n_F = k_F^3/(3\pi^2)$ . This standard result [26] showing that  $T_{BEC}$  is proportional to the Fermi energy  $E_F$  is not surprising since each of the molecular bound states are formed of two fermions.

In the anisotropic case, when artificial spin-orbit and Zeeman fields are present, the only modification in the intermediate expression for the Bose-Einstein condensation temperature shown above is to change the mass  $M$  of the bound-state into the geometrical mean  $M_{gm} = (M_x M_y M_z)^{1/3}$ , leading to the result

$$T_{BEC} = \frac{1}{C^{2/3}} \frac{n_{bs}^{2/3}}{M_{gm}}. \quad (35)$$

If we define the condensation temperatures of the anisotropic and isotropic cases to be  $T_{BEC}^{ani}$  and  $T_{BEC}^{iso}$ , respectively, then their ratio is simply given by

$$\frac{T_{BEC}^{ani}}{T_{BEC}^{iso}} = \frac{M}{M_{gm}}. \quad (36)$$

This result shows that if the mass  $M_{gm}$  is smaller than  $M$  then  $T_{BEC}^{ani}$  is larger than  $T_{BEC}^{iso}$  and vice-versa. In the limit that the interaction parameter is much larger than the appropriately scaled artificial spin-orbit coupling and Zeeman fields, the effective masses become isotropic, and the standard results are recovered, as expected.

In terms of the Fermi energy  $E_F$ , the condensation temperature for the anisotropic case becomes

$$\frac{T_{BEC}^{ani}}{E_F} = 0.218 \frac{2m}{M_{gm}}, \quad (37)$$

which again shows that an enhancement in the condensation temperature of Feshbach molecules in the presence of spin-orbit coupling is possible provided that the effective mass  $M_{gm}$  is smaller than twice the fermion mass. In the equal-Rashba-Dresselhaus case, the geometrical mean mass is  $M_{gm} = (2m)^{2/3} (M_x)^{1/3}$ , since  $M_y = M_z = 2m$  and Eq. (37) reduces to the relation  $T_{BEC}^{ani}/E_F = 0.218 [(2m)/M_x]^{1/3}$ . However, in the Rashba case, the geometrical mean mass is  $M_{gm} = (2m)^{1/3} (M_R)^{2/3}$ , since  $M_x = M_y = M_R$ , and  $M_z = 2m$ , leading to  $T_{BEC}^{ani}/E_F = 0.218 [(2m)/M_R]^{2/3}$ .

Having briefly discussed Bose-Einstein condensation of Feshbach molecules when spin-orbit and Zeeman fields are present, we are ready to present next our conclusions.

## V. CONCLUSIONS

We have investigated the emergence of Feshbach molecules in the presence of spin-orbit coupling and Zeeman fields for any mixture of Rashba and Dresselhaus terms in two and three dimensions, but we focused on the

experimentally relevant case of equal Rashba and Dresselhaus (ERD) spin-orbit coupling for three-dimensional systems.

For zero detuning ( $h_y = 0$ ) and fixed ERD spin-orbit coupling, we have found that the threshold scattering parameter [ $1/(k_F a_s, th)$ ], required to form Feshbach molecules with zero center-of-mass (CM) momentum, is shifted to larger positive values when the Raman coupling ( $h_z$ ) is increased. Furthermore, for fixed scattering parameter [ $1/(k_F a_s)$ ], these molecules are stable only for a symmetric range of CM momenta, outside which they decay into the two-particle continuum.

However, for finite detuning ( $h_y \neq 0$ ) and fixed Raman intensity, ERD spin-orbit coupling and scattering parameter, Feshbach molecules are stable only in an asymmetric range of CM momenta. Furthermore, if the detuning is sufficiently large then Feshbach molecules with zero CM momentum are not possible. These effects are a manifesta-

tion of the absence of Galilean invariance and the loss of parity.

Lastly, we have briefly discussed that spin-orbit coupling and Zeeman fields affect the Bose-Einstein condensation temperature of Feshbach molecules through the emergence of anisotropic effective masses, that is, the spin-orbit and Zeeman fields renormalize the masses of two-fermion bound states along the principal axes of their center of mass motion.

### Acknowledgments

We thank ARO (W911NF-09-1-0220) for support, Ian Spielman and Ross Williams for discussions, and Vijay Shenoy for alerting us to his related work [27].

- 
- [1] M. Z. Hasan and C. L. Kane, *Rev. Mod. Phys.* **82**, 3045 (2010).
- [2] X. L. Qi and S. C. Zhang, *Rev. Mod. Phys.* **83**, 1057 (2011).
- [3] Y. J. Lin, K. Jimenez-Garcia, and I. B. Spielman, *Nature* **471**, 83 (2011).
- [4] M. Chapman, and C. Sá de Melo, *Nature* **471**, 41 (2011).
- [5] J. P. Vyasankere, S. Zhang, and V. B. Shenoy, *Phys. Rev. B* **84**, 014512 (2011).
- [6] M. Gong, S. Tewari, and C. Zhang, *Phys. Rev. Lett.* **107**, 195303 (2011).
- [7] Z.-Q. Yu and H. Zhai, *Phys. Rev. Lett.* **107**, 195305 (2011).
- [8] H. Hu, L. Jiang, X.-J. Liu, and H. Pu, *Phys. Rev. Lett.* **107**, 195304 (2011).
- [9] S. Sinha, R. Nath, and L. Santos, *Phys. Rev. Lett.* **107**, 270401 (2011).
- [10] T. Ozawa, and G. Baym, *Phys. Rev. Lett.* **110**, 085304 (2013).
- [11] J. Dalibard, F. Gerbier, G. Juzeliunas, and P. Ohberg, *Rev. Mod. Phys.* **83**, 1523 (2011).
- [12] T. L. Ho and S. Zhang, *Phys. Rev. Lett.* **107**, 150403 (2011).
- [13] Y. Li, L. P. Pitaevskii, S. Stringari, *Phys. Rev. Lett.* **108**, 225301 (2012).
- [14] L. Han, and C. A. R. Sá de Melo, *Physical Review A* **85**, 011606 (R) (2012).
- [15] K. Seo, L. Han, and C. A. R. Sá de Melo, *Phys. Rev. A* **85**, 033601 (2012).
- [16] K. Seo, L. Han, and C. A. R. Sá de Melo, *Phys. Rev. Lett.* **109**, 105303 (2012).
- [17] C. Chin, R. Grimm, P. Julienne, and E. Tiesinga, *Rev. Mod. Phys.* **82**, 1225 (2010).
- [18] C. A. Regal, C. Ticknor, J. L. Bohn, and D. S. Jin, *Nature* **424**, 47 (2003).
- [19] M. Greiner, C. A. Regal, and D. S. Jin, *Nature* **426**, 537 (2003).
- [20] S. Jochim, M. Bartenstein, A. Altmeyer, G. Hendl, S. Riedl, C. Chin, J. Hecker Denschlag, and R. Grimm *Science* **302**, 2101 (2003).
- [21] P. Wang, Z.-Q. Yu, Z. Fu, J. Miao, L. Huang, S. Chai, H. Zhai, and J. Zhang, *Phys. Rev. Lett.* **109**, 095301 (2012).
- [22] L. W. Cheuk, A. T. Sommer, Z. Hadzibabic, T. Yefsah, W. S. Bakr, and M. W. Zwierlein, *Phys. Rev. Lett.* **109**, 095302 (2012).
- [23] R. A. Williams, M. C. Beeler, L. J. LeBlanc, K. Jiménez-García and I. B. Spielman, *Phys. Rev. Lett.* **111**, 095301 (2013) See also arXiv:1306.1965v1 (2013).
- [24] Zhengkun Fu, Lianghai Huang, Zengming Meng, Pengjun Wang, Long Zhang, Shizhong Zhang, Hui Zhai, Peng Zhang and Jing Zhang, *Nature Physics* **10**, 110 (2014). See also arXiv:1306.4568v2 (2013).
- [25] D. M. Kurcuoglu and C. A. R. Sá de Melo, arXiv:1306.1964v1 (2013), and D. M. Kurcuoglu, Ph. D. Thesis (2015).
- [26] C. A. R. Sá de Melo, M. Randeria, J. R. Engelbrecht, *Phys. Rev. Lett.* **71**, 3202 (1993).
- [27] V. B. Shenoy, *Phys. Rev. A* **88**, 033609 (2013). See also arXiv:1211.1831v1 (2012).